Physics Letters B 814 (2021) 136062

Contents lists available at ScienceDirect

Physics Letters B

www.elsevier.com/locate/physletb

Probing entrance channel effects in fusion-fission dynamics through neutron multiplicity measurement of ^{208}Rn

Neeraj Kumar [a,*], Shashi Verma [a], Shabnam Mohsina [b,c], Jhilam Sadhukhan [b,c], K. Rojeeta Devi [a,1], A. Banerjee [a,2], N. Saneesh [d], M. Kumar [d], Ruchi Mahajan [e], Meenu Thakur [e,3], Gurpreet Kaur [e,4], Anjali Rani [a], Neelam [a], Abhishek Yadav [d], Kavita [f], Rakesh Kumar [f], Unnati [a], S. Mandal [a], Suresh Kumar [a], B.R. Behera [e], K.S. Golda [d], A. Jhingan [d], P. Sugathan [d]

[a] Department of Physics & Astrophysics, University of Delhi, Delhi-110007, India
[b] Physics Group, Variable Energy Cyclotron Centre, Kolkata 700064, India
[c] Homi Bhabha National Institute, Training School Complex, Anushakti Nagar, Mumbai 400094, India
[d] Inter University Accelerator Centre, Aruna Asaf Ali Marg, New Delhi-110067, India
[e] Department of Physics, Panjab University, Chandigarh-160014, India
[f] Department of Physics, Kurukshetra University, Kurukshetra-136119, India

ARTICLE INFO

Article history:
Received 2 June 2020
Received in revised form 16 December 2020
Accepted 1 January 2021
Available online 7 January 2021
Editor: D.F. Geesaman

Keywords:
Nuclear fission dynamics
Neutron multiplicity
Dynamical model calculations

ABSTRACT

The pre- and post-scission neutron multiplicities are measured for the fission of ^{208}Rn, populated with the reactions ^{30}Si+^{178}Hf and ^{48}Ti+^{160}Gd in the excitation energy range of 54.5 - 80.8 MeV. We found significant differences in the pre-scission neutron multiplicities of these two systems. Also, both the reactions exhibit an enhancement in the pre-scission multiplicity with respect to the existing data for the ^{16}O+^{194}Pt reaction populating ^{210}Rn. The measured multiplicities are compared with the theoretical predictions obtained from the Langevin dynamical model for fission. Dynamical simulations are also performed to estimate the capture cross-sections. Contribution of the neutrons, emitted during the fusion process, is shown to be crucial in determining the neutron multiplicities for the present systems. Moreover, in case of the ^{48}Ti+^{160}Gd reaction, rapid quasi-fission dynamics prevents neutron emission from the thermalized target-projectile composite. The present measurement helps us to understand the relative importance of fusion and quasi-fission processes and their timescales depending on the entrance channel mass asymmetry.

1. Introduction

In heavy-ion induced reactions, the formation and decay of an equilibrated compound nucleus (CN) involve intricate many-body dynamics. Both measurement and modeling of these complex dynamical processes are under investigation for many decades. Probes like multiplicities of neutrons [1–3], charged particles [4,5], and γ-ray [6–8] are widely used to understand the fusion-fission (FF) dynamics. Among these observables, neutron emission is the dominant decay mode when the excitation energy of a compound system is sufficiently high. It occurs at various stages of the reaction dynamics and provides the information of these different dynamical phases [9–19]. For example, measurement of pre-scission neutron multiplicity (n_{pre}) reveals the importance of nuclear dissipation that can be incorporated within a suitable dynamical model [20–22] for compound nuclear decay. Further, n_{pre} may contain neutrons emitted during fusion, *i.e.* in the course of CN formation, if the associated dynamical evolution is slow enough and the emission is energetically admissible.

The dynamical time and the corresponding outcome strongly depend on the entrance channel mass asymmetry $\alpha = (A_T - A_P)/(A_T + A_P)$, where A_T and A_P are the masses of the target and projectile nuclei, respectively. Initially, a thermalized dinuclear

* Corresponding author.
E-mail address: neerajkumar.phys@gmail.com (N. Kumar).
[1] Presently at Inter University Accelerator Centre, Aruna Asaf Ali Marg, New Delhi-110067, India.
[2] Presently at GSI Helmholtzzentrum für Schwerionenforschung, Planckstrasse 1, 64291 Darmstadt, Germany.
[3] Presently at Department of Physics and Astrophysics, Central University of Haryana, Jant-Pali, Mahendergarh, Haryana-123031, India.
[4] Presently at Instituto de Física, Universidade de São Paulo, Rua do Matao, 1371, 05508-090 São Paulo, Brazil.

https://doi.org/10.1016/j.physletb.2021.136062

composite is formed through capture of target and projectile. For a sufficiently large value of α, the composite then experiences a strong driving force towards a compact compound nuclear configuration and it rapidly fuses to a fully equilibrated CN. However, in case of a smaller α, the CN formation (fusion) time may become long enough that allows neutron emission. Especially, for a more symmetric ($\alpha < \alpha_{\rm fus}$) composite, the mass-equilibration process is hindered by the fusion barrier, located at $\alpha = \alpha_{\rm fus}$, and the system may prefer to re-separate without attaining the full equilibration. Such a non-compound decay, known as quasi-fission (QF) process, is usually faster than the total FF timescale and, therefore, it suppresses the overall neutron yield. All the neutrons, emitted after the formation of a thermalized dinuclear composite and until the composite bifurcates, are accounted in n_{pre}. It means, apart from pre-scission neutrons, n_{pre} includes neutrons emitted during the QF decay.

The total evolution time of a thermalized composite is directly correlated to n_{pre} and, under energetically favorable conditions, more neutrons are expected to be emitted when the composite takes a longer time to reach scission. Various measurements of n_{pre} have been performed to investigate the fission timescales [23–26]. Also, neutron emission during the formation of a CN is conjectured in different n_{pre} measurements [24,27,28]. However, similar measurements to address the role of α in different entrance channel reaction mechanisms is absent. The present work provides the scope to understand the FF and QF processes through their timescales by utilizing n_{pre} as a clock. We measured n_{pre} for two different reactions ^{30}Si+^{178}Hf ($\alpha = 0.71$) and ^{48}Ti+^{160}Gd ($\alpha = 0.54$) at similar excitation energies ranging from 54.5 to 80.8 MeV. Both the entrance channels populate the same CN: ^{208}Rn. Results are compared with the n_{pre} data [29] of the ^{16}O+^{194}Pt reaction that populates a nearby isotope (^{210}Rn). It is observed that QF, fast-fission [30] and per-equilibrium fission [31] events are negligible for this reaction, indicating the presence of only FF decay. Moreover, these experimental results suggest the absence of any considerable fusion delay and, thus, the corresponding formation time for such an asymmetric entrance channel is assumed to be negligible in respect to any neutron evaporation. The above considerations regarding the ^{16}O+^{194}Pt reaction are explained qualitatively by using the entrance channel potential energy surface (PES). Here theoretical analyses are performed by using stochastic Langevin dynamical models at various stages of the time evolution. First, the capture cross-sections for the present reactions are estimated with a two-dimensional Langevin model. Then, the compound nuclear decay is studied with the Langevin dynamical model for fission, where the dissipation strength is adjusted to reproduce the experimental n_{pre} for our reference system of ^{16}O+^{194}Pt from which the neutron emission is neglected during fusion.

2. Experimental details

We performed the experiment at the National Array of Neutron Detectors (NAND) [32] facility of IUAC, New Delhi, using pulsed beams of ^{30}Si and ^{48}Ti from the 15UD Pelletron accelerator + LINAC booster. Both the beams had repetition rate of 250 ns with a beam width of ∼800 ps. We used targets of carbon backed ^{178}Hf (thickness ∼350 μg/cm^2) and self-supporting ^{160}Gd (thickness ∼1.00 mg/cm^2). A schematic of the experimental setup is shown in Fig. 1. To detect the complementary fission fragments in coincidence with each other, we placed two multi-wired proportional counters (MWPCs) [33] symmetrically at angles (θ_{lab}, ϕ_{lab}) of (69°, 90°) and (−69°, 270°) for ^{30}Si+^{178}Hf, and (59°, 90°) and (−59°, 270°) for ^{48}Ti+^{160}Gd. Each MWPC has an active area of 11 × 16 cm^2 and were maintained at an effective distance of 16.5 cm from the target. Angular coverages provided by the MWPCs

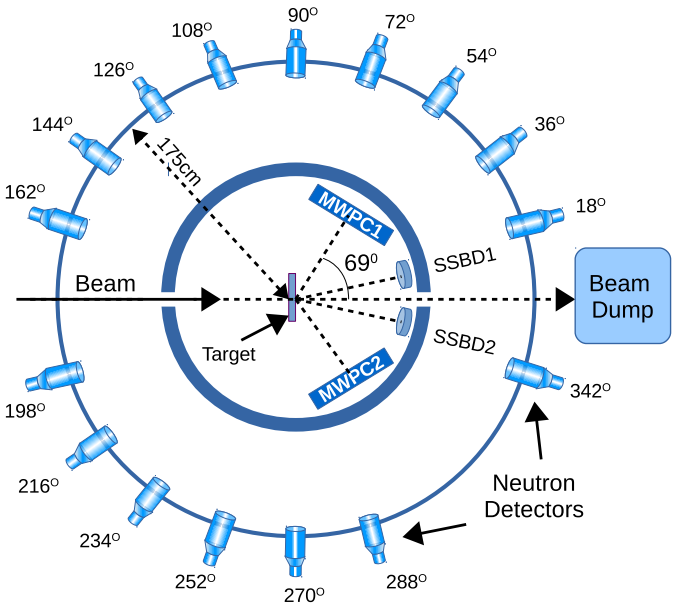

Fig. 1. (Color online) Experimental setup (top view) used for measurement of neutron multiplicity in coincidence with fission fragments. Two MWPCs, two monitor detectors (SSBD1 and SSBD2) and neutron detectors are placed in the reaction plane for ^{30}Si+^{178}Hf.

were ±18.4° along θ_{lab} and ±25.9° along ϕ_{lab}. Timing and position resolutions of these detectors were ∼1 ns and ∼1.2 mm, respectively. We operated the detectors at 3.0 mbar pressure of isobutane gas and a cathode bias of −420 V. We detected the neutrons, in coincidence with the fission fragments, by using an array [34,35] of 100 organic liquid scintillator detectors BC501A (5″ × 5″) coupled to PMT-R4144. Total solid angle coverage of this detector-array is 3.3% of 4π. A hardware threshold of 120 keVee [36] is determined by calibrating these neutron detectors with γ-rays from ^{137}Cs, ^{60}Co, and ^{22}Na radioactive sources. We coupled a VME based data acquisition system with the Linux Advanced Multi-Parameter System (LAMPS) [37] software to acquire the event mode data. The acquisition is set according to a trigger logic generated by coincidence between the RF of the beam pulse and the fission detectors. A beam dump was placed at a distance of 4 m from the target and shielded with thick layers of lead and borated paraffin in order to prevent any unnecessary background radiation [38]. We recorded the time-of-flight (TOF) signals from the neutron detectors. These detectors can sense neutrons as well as γ-rays. Therefore, to distinguish these two types of signals, pulse-shape discrimination (PSD) modules, based on the zero crossover technique, were used [39] with the TOF spectra. Efficiency of the neutron detectors is calibrated by measuring [40] the neutron spectrum of the well-known ^{252}Cf source and then comparing it with the simulated results from FLUKA [41], which is a multi-particle transport code based on the Monte-Carlo method.

3. Data analysis and results

Data analysis is performed using the LAMPS and ROOT packages. Two-dimensional correlated TOF spectra, as shown in Fig. 2(a), are generated from fast timing signals of the two MWPCs and used to separate the fission events from all possible contamination. To filter γ-rays from neutrons, a TOF-PSD neutron gate (shown by the dashed loop in Fig. 2 (b)) is applied on the TOF spectra. The peak position of the prompt γ-ray is used to calibrate the time of each TOF spectrum. These calibrated TOF spectra were then converted into the neutron energy spectra where the energy of a neutron is given by $E_n = 0.5 \times m_n\,(l/TOF)^2$ (in J); m_n being

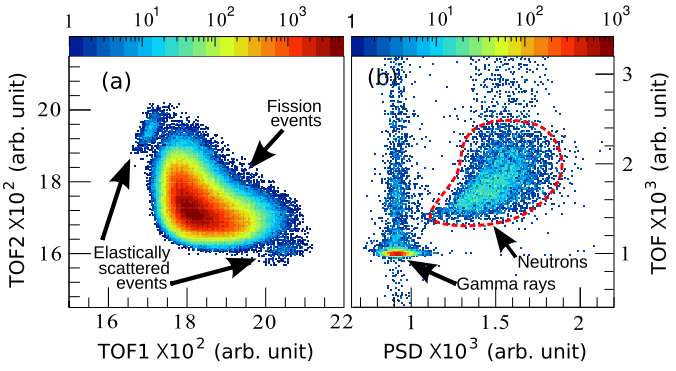

Fig. 2. (Color online) (a) Time correlation spectra of complementary fission fragments detected in the MWPCs, (b) PSD versus TOF spectrum of a neutron detector, for ^{30}Si+^{178}Hf, measured at E* = 79.4 MeV.

the mass of a neutron and $l = 175$ cm, is the length of the flight path. Angular uncertainties, imposed by the large area of the fission detectors, are reduced by dividing the position spectrum of each MWPC into four equal sectors. Subsequently, each neutron TOF spectrum is split into four components by applying the MWPC position gates. The energy spectra are binned in intervals of 0.5 MeV and energy dependent efficiency corrections are applied to obtain the neutron counts in all the neutron detectors. Then, to extract the double differential neutron multiplicities (DDNMs), the efficiency-corrected energy spectra are further normalized with the corresponding acceptance (solid angle) of the neutron detectors and the number of fission events. The pre- and post-scission neutrons can be separated by employing the multiple-source (CN and two fission fragments) least-square fitting procedure to all of the DDNM spectra, simultaneously. The fitting equation is given by [42],

$$\frac{d^2n}{dE_n d\Omega_n} = \sum_{i=1}^{3} \frac{n_i\sqrt{E_n}}{2(\pi T_i)^{3/2}} \times \exp\left[-\frac{E_n - 2\sqrt{E_n \frac{E_i}{A_i}}\cos\theta_i + \frac{E_i}{A_i}}{T_i}\right], \tag{1}$$

where E_i, A_i, T_i, θ_i, and n_i are the kinetic energy, atomic number, temperature, detection angle, and multiplicity of the corresponding source, respectively. Multiplicity n_1 corresponds to the neutrons emitted before the scission *i.e.*, n_{pre}, and n_2 $(= n_3)$ is the multiplicity of neutrons emitted from a fission fragment *i.e.*, n_{post}. Therefore, the total multiplicity is $n_{total} = n_{pre} + 2n_{post}$. In Eq. (1), n_{pre} and n_{post}, and the respective temperatures are considered as free parameters. The kinetic energy of a fission fragment, E_2 (or E_3) is calculated from the Viola systematics for symmetric fragmentation [43]. The angular position of each MWPC sector is taken into account while calculating the angle between the source and a particular neutron detector. Fig. 3 shows some of the measured DDNM spectra along with the fitted n_{pre} and n_{post} components obtained at various detection angles. As expected, the n_{pre} spectra are almost isotropic (independent of the detection angle) and the n_{post} distributions are peaked along the directions of fission fragments, *i.e.*, for θ_{nf_1} or θ_{nf_2} (angles between a neutron detector and fission fragments) close to zero. Extracted best-fit values of n_{pre}, n_{post}, and n_{total} are given in Table 1. n_{pre} for the less symmetric system, ^{30}Si+^{178}Hf, is found to be higher than the more symmetric ^{48}Ti+^{160}Gd reaction.

Table 1
Extracted values of n_{pre}, $2n_{post}$, n_{total} for ^{30}Si+^{178}Hf and ^{48}Ti+^{160}Gd system at different excitation energy.

System	E^*(MeV)	n_{pre}	$2n_{post}$	n_{total}
^{30}Si + ^{178}Hf	54.5	2.76 ± 0.07	1.54 ± 0.04	4.30 ± 0.08
	59.6	3.08 ± 0.07	1.58 ± 0.04	4.66 ± 0.08
	64.8	3.22 ± 0.07	1.73 ± 0.04	4.95 ± 0.08
	69.1	3.58 ± 0.07	1.83 ± 0.04	5.41 ± 0.08
	74.2	3.80 ± 0.08	1.85 ± 0.05	5.65 ± 0.09
	79.4	3.94 ± 0.08	1.86 ± 0.05	5.80 ± 0.09
^{48}Ti + ^{160}Gd	56.0	2.37 ± 0.08	1.59 ± 0.05	3.96 ± 0.10
	61.4	2.69 ± 0.07	1.45 ± 0.04	4.14 ± 0.08
	66.1	2.78 ± 0.06	1.81 ± 0.04	4.59 ± 0.07
	70.7	2.97 ± 0.06	1.92 ± 0.04	4.89 ± 0.07
	76.2	3.33 ± 0.07	1.73 ± 0.04	5.06 ± 0.08
	80.8	3.45 ± 0.07	2.04 ± 0.04	5.49 ± 0.08

4. Theoretical analysis

Heavy-ion induced reactions can be visualized as three successive dynamical evolutions beginning with the formation of a thermalized dinuclear composite through capture. Then, the composite either decays via QF or evolves to a fully equilibrated CN. Finally, the CN either undergoes fission or stabilizes to an evaporation residue following light-particles and γ-ray evaporations. According to the compound-nuclear reaction theory, n_{pre} should be independent of the entrance channel provided neutron-evaporation occurs only after the formation of a CN with a particular angular momentum (ℓ) and excitation energy (E^*). Therefore, for the three reactions considered in the present work, we expect similar values of n_{pre} if the above conditions are fulfilled. We compare the results with E^* as an independent variable (see Fig. 6). In order to eliminate the ℓ related uncertainty, we calculate the partial capture cross-section $(d\sigma_c/d\ell)$ by solving the two-dimensional Langevin equation [22,44] given by

$$\begin{aligned}
\frac{dp_R}{dt} &= \frac{\ell^2}{\mu R^3} - \frac{dV_{cap}(R)}{dR} - K_{RR}\frac{p_R}{\mu} + g_{RR}\Gamma_R(t),\\
\frac{dR}{dt} &= \frac{p_R}{\mu},\\
\frac{1}{R}\frac{d\ell}{dt} &= -K_{\theta\theta}\frac{\ell}{\mu R} + g_{\theta\theta}\Gamma_\theta(t),\\
\frac{d\theta}{dt} &= \frac{\ell}{\mu R^2},
\end{aligned} \tag{2}$$

where R defines the relative separation between the center of masses of the target and projectile and θ is the angle subtended by R on the beam axis. The possibility of mass transfer among the target and projectile nuclei was theoretically suggested to be negligible during capture [44]. p_R is the momentum conjugate to R and μ is the reduced mass of the composite. The driving potential $V_{cap}(R)$ is calculated by double-folding the effective Migdal interaction with nuclear densities [45,46]. Corrections for the Coulomb and rotational energies are also taken into account. K_{RR} and $K_{\theta\theta}$ are the coefficients of the dissipation tensor calculated within the surface-friction model [22]. The strength of the random force with coefficients g_{RR} and $g_{\theta\theta}$ is obtained from the dissipation tensor by using the fluctuation dissipation theorem. The time dependent part $\Gamma_i(t)$ follows the time-correlation property: $\langle\Gamma_i(t)\Gamma_i(t')\rangle = 2\delta(t-t')$. An ensemble of N_t Langevin trajectories are simulated for each combination of ℓ and E^* (or $E_{c.m.}$) and the resulting $d\sigma_c/d\ell$ is calculated from the equation:

$$\frac{d\sigma_c}{d\ell} = \frac{\pi\hbar^2(2\ell+1)}{2\mu E_{c.m.}}\frac{N_c(\ell)}{N_t} \tag{3}$$

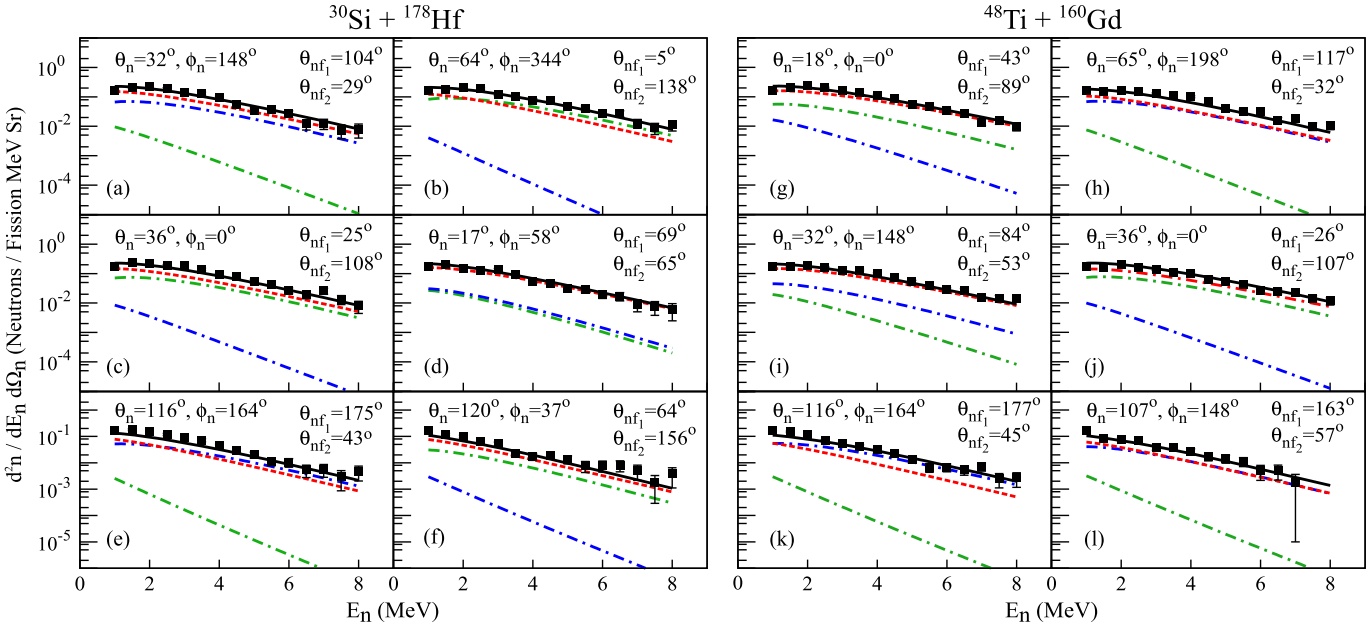

Fig. 3. (Color online) Double differential neutron multiplicity spectra for the reaction (a)-(f) ^{30}Si+^{178}Hf at $E^* = 79.4$ MeV and (g)-(l) ^{48}Ti+^{160}Gd at $E^* = 80.8$ MeV. θ_n and ϕ_n are polar and azimuthal angles of neutron detectors, θ_{nf_1} and θ_{nf_2} are angles between neutron detector and fission fragments. Symbols indicate measured data. n_{pre} (dashed line), n_{total} (solid line), and n_{post} (dash-dotted lines) from two fragments are obtained by fitting experimental values with Eq. (1).

where N_c is the number of captured events. A Langevin trajectory is considered to be a captured event when the radial kinetic energy along R is completely dissipated at a value of R inside the capture barrier [44]. Results are plotted in Fig. 4 along with the total capture cross-section (σ_c) obtained by integrating Eq. (3). The $d\sigma_c/d\ell$ distributions are considerably broader for the ^{30}Si and ^{48}Ti induced reactions compared to the ^{16}O case. It implies that these heavy projectiles produce high-ℓ composites in comparison to ^{16}O. Equivalently, at similar E^*, ^{48}Ti populates even higher values of ℓ than ^{30}Si. Next, two-dimensional PES is calculated along R and α as shown in Fig. 5. The liquid drop part of the PES is obtained by using the same Migdal interaction [45,46] and the shell corrections are added from experimental binding energies [47] for different dinuclear combinations. For all the three reactions, captured events form thermalized composites with configurations as indicated in Fig. 5. Subsequent evolution of these composites depends on the force exerted by the driving potential. Evidently, as

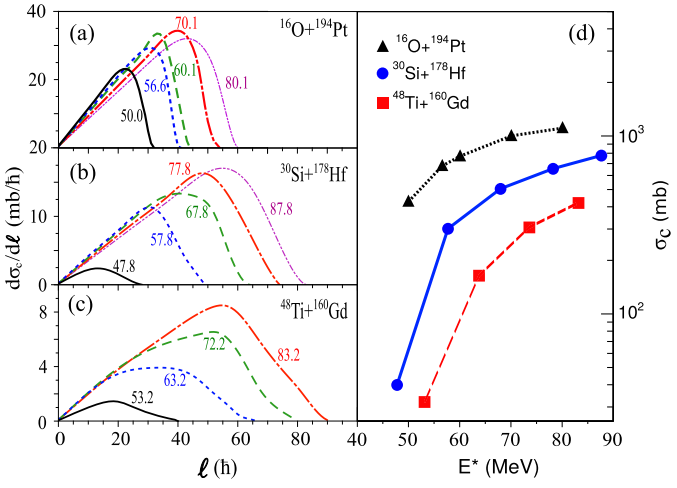

Fig. 4. (Color online) Left panels: variation of $d\sigma_c/d\ell$ with ℓ for different E^* (in MeV) as indicated on each curve. Reaction channels are mentioned in each panel. Right panel: Calculated σ_c from $d\sigma_c/d\ell$ curves.

discussed in section 1, the ^{16}O+^{194}Pt (although the calculated PES corresponds to ^{16}O+^{192}Pt, it is similar to the PES for ^{16}O+^{194}Pt) system achieves complete equilibration due to strong driving force towards $\alpha = 1$. The minima of the PES along the R direction are marked by a dashed line in Fig. 5. The maximum potential on this line is defined as the fusion barrier and the corresponding α is defined as α_{fus}. The relatively symmetric composite of ^{30}Si lies on the boundary of a shallow well that lies close to the fusion barrier and, therefore, it takes a longer time to reach the fusion pocket. Moreover, this system may decay via QF due to shape fluctuations triggered by the excitation energy of the system. In fact, in similar reactions, a weaker (∼10%) contribution from the slow QF process is predicted [48]. In contrast, for the ^{48}Ti+^{160}Gd reaction ($\alpha < \alpha_{fus}$), fast QF decay is energetically more favorable. The dominance of QF in ^{48}Ti induced reactions is observed in various experiments [49,50]. Interestingly, according to the PES, QF events prefer a pathway towards near-symmetric ($\alpha \approx 0.1$) fragmentation and this can not be distinguished experimentally from the fission fragment mass distribution, apart from a broadening in the distribution. It ensures the presence of QF neutrons in our measured n_{pre}. We want to mention that the mass-angle correlations of fission fragments are also measured for the present reactions and the analysis is underway to distinguish QF and FF events.

Next, we calculate n_{pre} by presuming that all the captured events emerge to compound nuclei without any formation delay *i.e.* the evolution of the dinuclear shape to a CN is pretty fast. Although this assumption is thought to be valid for the reference reaction and not to be true for our measurements. We perform this calculation to isolate the non-compound contributions in n_{pre}. We solve Langevin dynamics for fission to simulate the time-evolution for an ensemble of compound nuclei. The initial ℓ is sampled from the $d\sigma_c/d\ell$ distributions given in Fig. 4. The Langevin equation for the Hill-Wheeler elongation coordinate c [51] can be written as [21],

$$\frac{dp}{dt} = \frac{p^2}{2}\frac{d}{dc}\left(\frac{1}{\mathcal{M}}\right) - \frac{dF(c)}{dc} - \beta p + g\Gamma(t),$$
$$\frac{dc}{dt} = \frac{p}{\mathcal{M}} \qquad (4)$$

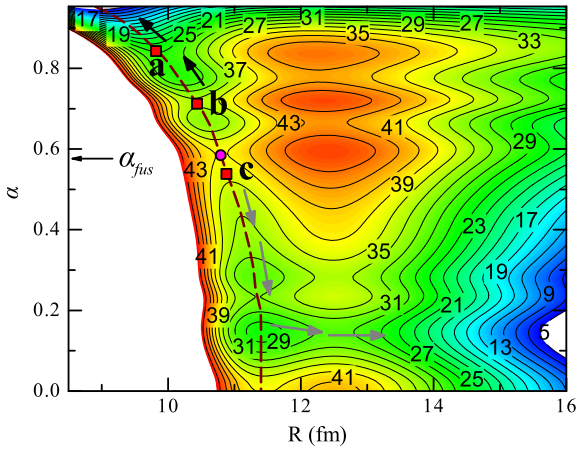

Fig. 5. (Color online) Potential energy surface (in MeV) as a function of R and α (see text). Square symbols 'a', 'b', and 'c' are the configurations of thermalized composites formed after the capture process in reactions ^{16}O+^{194}Pt, ^{30}Si+^{178}Hf, and ^{48}Ti+^{160}Gd, respectively. The dashed line defines potential minima along R and the circle indicates the location of the fusion barrier (α_{fus}). Probable decay routes are shown by black (FF path) and gray (QF path) arrows.

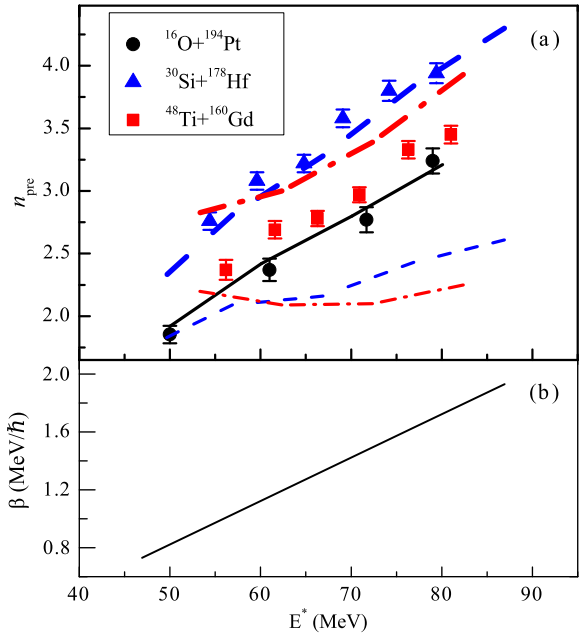

Fig. 6. (a) Measured n_{pre} for ^{30}Si+^{178}Hf (triangles), ^{48}Ti+^{160}Gd (squares), and existing data [29] for ^{16}O+^{194}Pt (circles) reactions. Thin lines are calculated n_{pre} for ^{30}Si+^{178}Hf (dashed lines), ^{48}Ti+^{160}Gd (dash-dotted lines), and ^{16}O+^{194} (solid lines) without formation delay. Thick lines correspond to $\tau = 65 \times 10^{-21}$ s. The β used for the dynamical calculations is shown in (b).

where $\mathcal{M}$ is the shape dependent collective inertia calculated within the Werner-Wheeler prescription [52] and p is the collective momentum. The strength of the random force g and the random number $\Gamma(t)$ are obtained in a similar way as described for Eq. (3). Helmholtz free energy, $F(c)$ is obtained from the double-folding Yukawa-plus-exponential potential [53] $V(c)$ as: $F(c) = V(c) - (a(c) - a(0))T^2$; $a(c)$ being the shape dependent level density parameter and T is the Fermi-gas temperature for the spherical shape. We consider deformation dependent shell and pairing energy corrections in $V(c)$. To this end, two-centered shell model [26] is solved and then the Strutinsky's prescription [54] is employed to extract the microscopic energy correction. Evaporation of neutron, proton, α-particle, and GDR γ-ray are considered at each Langevin time-step. Evaporation widths are calculated within the standard statistical model prescription [22,55]. The reduced dissipation strength β is used as a free parameter and it is adjusted independently for each E^* to reproduce the experimental n_{pre} for the reference reaction. Calculated n_{pre} and the β are plotted in Fig. 6. Further, β must be independent of the formation channel. Hence, we use the same β to calculate n_{pre} for the other two reactions. As shown in Fig. 6, calculated n_{pre} (thin lines) for these reactions are below the values corresponding to the reference reaction. This is in agreement with our expectation since a higher compound nuclear ℓ, produced in case of our systems as explained above, effectively reduces the fission barrier and makes the fission process faster. As a result, the chances of neutron evaporation diminishes.

The finding just described suggests that the neutrons emitted during the fusion process contributes substantially in n_{pre} for heavy projectiles. Specifically, for the ^{30}Si induced reaction, where the probability QF is low, observed excess neutrons are produced during the CN formation. The presence of a long CN formation time for ^{30}Si induced reaction is already predicted with the help of Fig. 5. Further, we repeated the Langevin calculation by incorporating a formation delay (or equivalently fusion-delay) τ. During this course of time, particle and γ-ray evaporations are allowed without any shape evolution. As shown in Fig. 6, $\tau = 65 \times 10^{-21}$ s is required to compensate for the excess neutrons. Moreover, this constant τ precisely reproduces the E^* dependence of the observed n_{pre}. However, the magnitude of τ is model dependent as it is directly correlated to the calculated neutron emission width. Also, an appropriate dynamical calculation, including real-time evolution of a dinuclear composite to a compound nuclear configuration, may predict τ more comprehensively. For the ^{48}Ti induced reaction, τ will be even higher. Therefore, we would have observed n_{pre} even higher than the ^{30}Si case if the composite were predominantly decayed via the FF route. However, as explained above, fast QF process dominates for this reaction channel. Consequently, overall neutron number decreases considerably and, even with $\tau = 65 \times 10^{-21}$ s, theoretical prediction overestimates the experimental n_{pre}. Ideally, for a more precise understanding, QF dynamics is required to be simulated in presence of neutron evaporations, which is beyond the scope of the present study.

5. Conclusion

To examine the role of entrance channel dynamics in heavy-ion induced reactions, we measured neutron multiplicities for the CN ^{208}Rn populated via two reactions, ^{30}Si + ^{178}Hf and ^{48}Ti + ^{160}Gd, having different mass asymmetry. Neutron multiplicities are found to be strongly influenced by the collective dynamics happening during the fusion and quasi-fission processes. Moreover, two distinct scenarios arise for the two entrance channels. The ^{30}Si induced reaction spends a considerable time in the fusion process before reaching the complete equilibration. On the other hand, for the ^{48}Ti case, fast quasi-fission decay plays a dominant role in the reaction dynamics. Present measurement effectively disentangles these two reaction mechanisms which involve different timescales. However, the neutron multiplicity probe is insensitive to the non-equilibrium processes that survive for a time period similar to the fusion-fission timescale. Study of other observables like mass distributions and mass-angle correlations of the fragments are necessary for a deeper understanding and work is in progress along this direction.

Declaration of competing interest

The authors wish to confirm that there are no known associated conflicts of interest or personal relationships that could have appeared to influence the work reported in this manuscript.

Acknowledgements

Authors acknowledge the Pelletron group and Target Laboratory of IUAC for their support during the experiments. One of the authors (N.K.), acknowledges the financial assistance provided by CSIR and IUAC, in the form of Senior Research Fellowship [09/045(1567)/2018-EMR-I] and Project Fellowship (UFR-52305), respectively. S.V. acknowledges the support of the University of Delhi in the form of R&D Grant.

References

[1] D.J. Hinde, D. Hilscher, H. Rossner, B. Gebauer, M. Lehmann, M. Wilpert, Phys. Rev. C 45 (1992) 1229.
[2] H. Rossner, D. Hilscher, D.J. Hinde, B. Gebauer, M. Lehmann, M. Wilpert, E. Mordhorst, Phys. Rev. C 40 (1989) 2629.
[3] J.O. Newton, Pramana 33 (1989) 175.
[4] J.P. Lestone, Phys. Rev. C 70 (1993) 2245.
[5] J.P. Lestone, J.R. Leigh, J.O. Newton, D.J. Hinde, J.X. Wei, J.X. Chen, S. Elfström, M. Zielinska-Pfabé, Nucl. Phys. A 559 (1993) 277.
[6] M. Thoennessen, D.R. Chakrabarty, M.G. Herman, R. Butsch, P. Paul, Phys. Rev. Lett. 59 (1987) 2860.
[7] R. Butsch, M. Thoennessen, D.R. Chakrabarty, M.G. Herman, P. Paul, Phys. Rev. C 41 (1990) 1530.
[8] D.J. Hofman, B.B. Back, P. Paul, Phys. Rev. C 51 (1995) 2597.
[9] D.J. Hinde, D. Hilscher, H. Rossner, Nucl. Phys. A 502 (1989) 497.
[10] D. Hilscher, H. Rossner, B. Cramer, B. Gebauer, U. Jahnke, M. Lehmann, E. Schwinn, M. Wilpert, Th. Wilpert, H. Frobeen, E. Mordhorst, W. Scobel, Phys. Rev. Lett. 62 (1989) 1099.
[11] Y. Aritomo, M. Ohta, T. Materna, F. Hanappe, O. Dorvaux, L. Stuttge, Nucl. Phys. A 759 (2005) 309.
[12] K. Banerjee, S. Bhattacharya, C. Bhattacharya, M. Gohil, S. Kundu, T.K. Rana, G. Mukherjee, R. Pandey, P. Roy, H. Pai, A. Dey, T.K. Ghosh, J.K. Meena, S. Mukhopadhyay, D. Pandit, S. Pal, S.R. Banerjee, Phys. Rev. C 85 (2012) 064310.
[13] Pratap Roy, K. Banerjee, C. Bhattacharya, R. Pandey, A. Sen, S. Manna, S. Kundu, T.K. Rana, T.K. Ghosh, G. Mukherjee, T. Roy, A. Dhal, A. Dey, J.K. Meena, A.K. Saha, Deepak Pandit, S. Mukhopadhyay, S. Bhattacharya, Phys. Rev. C 94 (2016) 064607.
[14] W. Ye, Phys. Rev. C 79 (2009) 031601(R).
[15] N. Wang, W. Ye, Phys. Rev. C 87 (2013) 051601(R).
[16] Jhilam Sadhukhan, Santanu Pal, Phys. Rev. C 78 (2008) 011603(R).
[17] Jhilam Sadhukhan, Santanu Pal, Phys. Rev. C 81 (2010) 031602(R).
[18] Varinderjit Singh, B.R. Behera, Maninder Kaur, A. Kumar, P. Sugathan, K.S. Golda, A. Jhingan, M.B. Chatterjee, R.K. Bhowmik, Davinder Siwal, S. Goyal, Jhilam Sadhukhan, Santanu Pal, A. Saxena, S. Santra, S. Kailas, Phys. Rev. C 87 (2013) 064601.
[19] D.J. Hinde, Nucl. Phys. A 553 (1993) 255.
[20] H.A. Kramers, Physica 7 (1940) 284.
[21] Y. Abe, S. Ayik, P.-G. Reinhard, E. Suraud, Phys. Rep. 275 (1996) 49.
[22] P. Fröbrich, I.I. Gontchar, Phys. Rep. 292 (1998) 131.
[23] D.J. Hinde, H. Ogata, M. Tanaka, T. Shimoda, N. Takahashi, A. Shinohara, S. Wakamatsu, K. Katori, H. Okamura, Phys. Rev. C 39 (1989) 2268.
[24] A. Saxena, A. Chatterjee, R.K. Choudhury, S.S. Kapoor, D.M. Nadkarni, Phys. Rev. C 49 (1994) 932.
[25] D. Jacquet, M. Morjean, Part. Nucl. Phys. 63 (2009) 155.
[26] M.T. Senthil Kannan, Jhilam Sadhukhan, B.K. Agrawal, M. Balasubramaniam, Santanu Pal, Phys. Rev. C 98 (2018) 021601(R).
[27] W.P. Zank, D. Hilscher, G. Ingold, U. Jahnke, M. Lehmann, H. Rossner, Phys. Rev. C 33 (1986) 519.
[28] J. Cabrera, Th. Keutgen, Y. El Masri, Ch. Dufauquez, V. Roberfroid, I. Tilquin, J. Van Mol, Phys. Rev. C 68 (2003) 034613.
[29] Rohit Sandal, B.R. Behera, Varinderjit Singh, Maninder Kaur, A. Kumar, G. Singh, K.P. Singh, P. Sugathan, A. Jhingan, K.S. Golda, M.B. Chatterjee, R.K. Bhowmik Sunil Kalkal, D. Siwal, S. Goyal, S. Mandal, E. Prasad, K. Mahata, A. Saxena, Jhilam Sadhukhan, Santanu Pal, Phys. Rev. C 87 (2013) 014604.
[30] E. Prasad, K.M. Varier, R.G. Thomas, P. Sugathan, A. Jhingan, N. Madhavan, B.R.S. Babu, Rohit Sandal, Sunil Kalkal, S. Appannababu, J. Gehlot, K.S. Golda, S. Nath, A.M. Vinodkumar, B.P. Ajith Kumar, B.V. John, Gayatri Mohanto, M.M. Musthafa, R. Singh, A.K. Sinha, S. Kailas, Phys. Rev. C 81 (2010) 054608.
[31] E. Prasad, K.M. Varier, R.G. Thomas, A.M. Vinod Kumar, K. Mahata, S. Appannababu, P. Sugathan, K.S. Golda, B.R.S. Babu, A. Saxena, B.V. John, S. Kailas, Nucl. Phys. A 882 (2012) 62.
[32] N. Saneesh, K.S. Golda, A. Jhingan, S. Venkataramanan, T. Varughese, Mohit Kumar, Meenu Thakur, Ruchi Mahajan, B.R. Behera, P. Sugathan, A. Chatterjee, M.B. Chatterjee, Nucl. Instrum. Methods Phys. Res. A 986 (2021) 164754.
[33] Akhil Jhingan, Gurpreet Kaur, N. Saneesh, Ruchi Mahajan, Meenu Thakur, Tathagata Banerjee, Rakesh Dubey, Priya Sharma, Abhishek Yadav, R. Ahuja, B.R. Behera, P. Sugathan, Proc. DAE Symp. Nucl. Phys. 60 (2015) 936.
[34] P. Sugathan, A. Jhingan, K.S. Golda, T. Varughese, S. Venkataramanan, N. Saneesh, V.V. Satyanarayana, S.K. Suman, J. Antony, R. Shanti, K. Singh, S.K. Saini, A. Gupta, A. Kothari, P. Barua, Rajesh Kumar, J. Zacharias, R.P. Singh, B.R. Behera, S.K. Mandal, I.M. Govil, R.K. Bhowmik, Pramana 83 (2014) 807.
[35] K.S. Golda, A. Jhingan, P. Sugathan, H. Singh, R.P. Singh, B.R. Behera, S. Mandal, A. Kothari, A. Gupta, J. Zacharias, M. Archunan, P. Barua, S. Venkataramanan, R.K. Bhowmik, I.M. Govil, S.K. Datta, M.B. Chatterjee, Nucl. Instrum. Methods Phys. Res. A 763 (2014) 58.
[36] T.G. Masterson, Nucl. Instrum. Methods 88 (1970) 61.
[37] Linux Advanced MultiParameter System, https://www.tifr.res.in/~pell/lamps.html, 2002.
[38] N. Saneesh, S.K. Saini, G. Mohanto, R.K. Dubey, A. Jhingan, P. Sugathan, Proc. DAE Symp. Nucl. Phys. 58 (2013) 952.
[39] S. Venkataramanan, Arti Gupta, K.S. Golda, Hardev Singh, Rakesh Kumar, R.P. Singh, R.K. Bhowmik, Nucl. Instrum. Methods Phys. Res. A 596 (2008) 248.
[40] Ruchi Mahajan, B.R. Behera, Meenu Thakur, Gurpreet Kaur, Priya Sharma, Kushal Kapoor, A. Kumar, P. Sugathan, A. Jhingan, A. Chatterjee, N. Saneesh, A. Yadav, R. Dubey, Neeraj Kumar, Hardev Singh, A. Saxena, Santanu Pal, Phys. Rev. C 98 (2018) 034601.
[41] A. Ferrari, P.R. Sala, A. Fasso, J. Ranft, FLUKA: a Multi particle Transport Code, Reports No. CERN-2005-10, No. INFN/TC 05/11, and No. SLAC-R-773, 2005, https://www.slac.stanford.edu/pubs/slacreports/reports16/slac-r-773.pdf.
[42] D. Hilscher, J.R. Birkelund, A.D. Hoover, W.U. Schröder, W.W. Wilcke, J.R. Huizenga, A.C. Mignerey, K.L. Wolf, H.F. Breuer, V.E. Viola Jr., Phys. Rev. C 20 (1979) 576.
[43] V.E. Viola, K. Kwiatkowski, M. Walker, Phys. Rev. C 31 (1985) 1550.
[44] Shabnam Mohsina, Jhilam Sadhukhan, Phys. Rev. C 101 (2020) 044607.
[45] Avazbek Nasirov, Akira Fukushima, Yuka Toyoshima, Yoshihiro Aritomo, Akhtam Muminov, Shuhrat Kalandarov, Ravshanbek Utamuratov, Nucl. Phys. A 759 (2005) 342.
[46] V. Zagrebaev, A. Karpov, Y. Aritomo, M. Naumenko, W. Greiner, Phys. Elem. Part. At. Nucl. 38 (2007) 469.
[47] W.D. Myers, W.J. Swiatecki, Nucl. Phys. 81 (1966) 1.
[48] A. Shamlath, M. Shareef, E. Prasad, P. Sugathan, R.G. Thomas, A. Jhingan, S. Appannababu, A.K. Nasirov, A.M. Vinodkumar, K.M. Varier, C. Yadav, B.R.S. Babu, S. Nath, G. Mohanto, Ish Mukul, D. Singh, S. Kailas, Nucl. Phys. A 945 (2016) 67.
[49] B.B. Back, P.B. Fernandez, B.G. Glagola, D. Henderson, S. Kaufman, J.G. Keller, S.J. Sanders, F. Videbæk, T.F. Wang, B.D. Wilkins, Phys. Rev. C 53 (1996) 1734.
[50] K. Banerjee, D.J. Hinde, M. Dasgupta, E.C. Simpson, D.Y. Jeung, C. Simenel, B.M.A. Swinton-Bland, E. Williams, I.P. Carter, K.J. Cook, H.M. David, Ch.E. Düllmann, J. Khuyagbaatar, B. Kindler, B. Lommel, E. Prasad, C. Sengupta, J.F. Smith, K. Vo-Phuoc, J. Walshe, A. Yakushev, Phys. Rev. Lett. 122 (2019) 232503.
[51] M. Brack, Jens Damgaard, A.S. Jensen, H.C. Pauli, V.M. Strutinsky, C.Y. Wong, Rev. Mod. Phys. 44 (1972) 320.
[52] K.T.R. Davies, A.J. Sierk, J.R. Nix, Phys. Rev. C 13 (1976) 2385.
[53] A.J. Sierk, Phys. Rev. C 33 (1986) 2039.
[54] V.M. Strutinsky, Nucl. Phys. A 122 (1968) 1.
[55] V. Weisskopf, Phys. Rev. 52 (1937) 295.